Kirwan, J. D., Bok, M. J., Smolka, J., Foster, J. J., Hernández, J. C., & Nilsson, D. E. (2018). The sea urchin Diadema africanum uses low resolution vision to find shelter and deter enemies. *Journal of Experimental Biology*, *221*(14), [jeb176271]. https://doi.org/10.1242/jeb.176271

© 2018. Published by The Company of Biologists Ltd | Journal of Experimental Biology (2018) 221, jeb176271. doi:10.1242/jeb.176271

RESEARCH ARTICLE

The sea urchin *Diadema africanum* uses low resolution vision to find shelter and deter enemies

John D. Kirwan[1], Michael J. Bok[1,2], Jochen Smolka[1], James J. Foster[1], José Carlos Hernández[3] and Dan-Eric Nilsson[1,*]

ABSTRACT

Many sea urchins can detect light on their body surface and some species are reported to possess image-resolving vision. Here, we measure the spatial resolution of vision in the long-spined sea urchin *Diadema africanum*, using two different visual responses: a taxis towards dark objects and an alarm response of spine-pointing towards looming stimuli. For the taxis response we used visual stimuli, which were isoluminant to the background, to discriminate spatial vision from phototaxis. Individual animals were placed in the centre of a cylindrical arena under bright down-welling light, with stimuli of varying angular width placed on the arena wall at alternating directions from the centre. We tracked the direction of movement of individual animals in relation to the stimuli to determine whether the animals oriented towards the stimulus. We found that *D. africanum* responds by taxis towards isoluminant stimuli with a spatial resolution in the range of 29–69 deg. This corresponds to a theoretical acceptance angle of 38–89 deg, assuming a contrast threshold of 10%. The visual acuity of the alarm response of *D. africanum* was tested by exposing animals to different sized dark looming and appearing stimuli on a monitor. We found that *D. africanum* displays a spine-pointing response to appearing black circles of 13–25 deg angular width, corresponding to an acceptance angle of 60–116 deg, assuming the same contrast threshold as above.

KEY WORDS: Visual acuity, Echinoidea, Photoreception, Sea urchin, Visual response, Visually guided behaviour

INTRODUCTION

Sea urchin adults are the only animals reported to possess resolving vision while, nonetheless, conspicuously lacking eyes. How sea urchin photodetection is mediated and what range of visual acuity is achieved have been previously explored (Millott and Yoshida, 1960; Yerramilli and Johnsen, 2010; Ullrich-Lüter et al., 2011) but are not categorically understood. Sea urchins (Echinoidea) are a large clade of echinoderms with diverse lifestyles but are predominantly night-active herbivores inhabiting shallow seas. Adult sea urchins are characterized by a globular endoskeleton (whose anatomical name is the 'test') comprising rows of adjoining calcareous plates (Fig. 1A). The test bears spines and is partitioned by five vertical fissures called ambulacra, around which tentacular 'tube feet' emerge. Directional photoreception, which is used for tasks such as shadow detection and alarm responses, can be achieved using one or a few photoreceptor cells, combined with the screening of off-axis light (Nilsson, 2009). Resolving vision (hereafter, vision), however, also uses information about the spatial distribution of ambient light and thereby allows for coordinated behavioural responses, such as object taxis and orientation in relation to spatial structures (see Nilsson, 2009 and Nilsson, 2013 for reviews of this topic).

Both directional photoreception and vision have been reported in echinoderms. Directional photoreception is widespread (Pearse and Arch, 1969; Yamamoto and Yoshida, 1978; Johnsen and Kier, 1999) and is mediated via receptors which may be dispersed or aggregated, such as the tentacular eyespots of synaptid holothurians (Yoshida et al., 1984). Moreover, vision has been reported in starfish via groups of ocelli (simple eyes) called 'optic cushions' at the arm tips (Garm and Nilsson, 2014; Petie et al., 2016). Coarse spatial vision via dispersed ocelli is also reported in chitons (Speiser et al., 2011) and possibly fan worms (Bok et al., 2016, 2017a,b). Sea urchins are therefore unusual in that, although they lack ocelli, they nonetheless exhibit coordinated and directed behaviours, which could rely on spatial vision, as described below.

A range of photic behaviours have been observed in sea urchins, including colour changes (Yoshida, 1956), spine reflexes and covering reactions (Millott, 1955; Lawrence, 1976). Sea urchins also exhibit coordinated photic behaviours, including defensive movements of the spines (Millott and Takahashi, 1963) and locomotion towards or away from light (Holmes, 1912; Yoshida, 1966), which necessitate a centralized response.

Extensive investigations of sea urchin photodetection have concerned spine-pointing responses of the genus *Diadema* (Yoshida et al., 1984). These diadematids are characterized by long, black spines and are abundant and ecologically important in tropical waters (Sammarco, 1980; Hernández et al., 2008). They are found primarily on shallow rocky and reef habitats (Hernández et al., 2008; Muthiga and McClanahan, 2013) from shallows to a depth of 70 m (Mortensen, 1940). *Diadema africanum* (Rodríguez et al., 2013) is a night-active (Tuya et al., 2004), herbivorous diadematid which occurs in the East Atlantic. It responds to a sudden decrease in light intensity, resulting in a jerking of spines on adjoining regions of the body surface, following illumination of the radial nerves in dissected sections of the calcareous skeleton (Yoshida and Millott, 1959). The spatial sensitivity profile of the spine-pointing response to light decrements coincides with the distribution of the superficial nerve network (Millott and Yoshida, 1960), and this has been taken as evidence of the direct, localized response of the superficial nerve network or associated receptors to photic stimuli. The response to dimming *in vivo* occurs as a

[1]Lund Vision Group, Department of Biology, Lund University, Lund 223 62, Sweden. [2]School of Biological Sciences, Faculty of Science, University of Bristol, Bristol BS8 1TH, UK. [3]Departamento de Biología Animal, Edafología y Geología (UD Ciencias Marinas), Universidad de La Laguna, Tenerife, Canary Islands, San Cristóbal de La Laguna 38200, Spain.

*Author for correspondence (dan-e.nilsson@biol.lu.se)

J.D.K., 0000-0001-5537-3574; M.J.B., 0000-0002-3169-8523; J.S., 0000-0003-2958-0697; J.J.F., 0000-0002-4444-2375; J.C.H., 0000-0002-1539-1783; D.-E.N., 0000-0003-1028-9314

Received 17 December 2017; Accepted 29 April 2018

Journal of Experimental Biology (2018) 221, jeb176271. doi:10.1242/jeb.176271

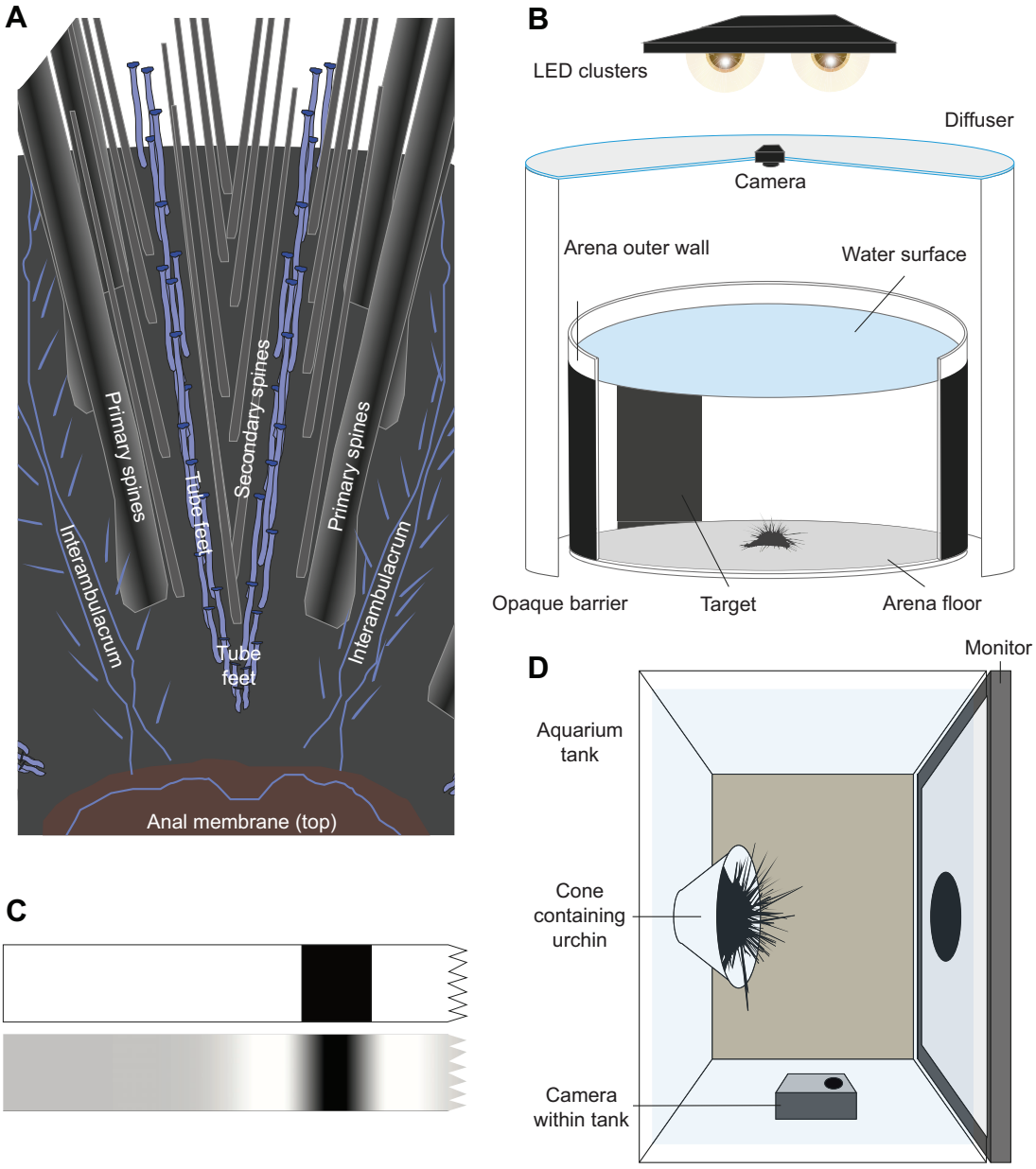

Fig. 1. *Diadema africanum* anatomy and the experimental design. (A) Superficial anatomy of *D. africanum*. (B) Diagram of behavioural setup for object taxis, with the near sectors of the arena wall and surrounding opaque barrier removed to view the inside of the arena. (C) Diagram of pattern types used to induce object taxis: a bar stimulus pattern (top) with a dark band subtending 40 deg, and a difference of Gaussians (DoG) stimulus pattern with a period of 69 deg (target half-width of 25 deg). (D) Diagram of behavioural setup for the spine-pointing response. Here, the stimulus is a computer monitor covering one side of the tank.

coordinated response following a delay, suggesting a neural coordination. It has been proposed on this basis that sea urchin vision occurs via a 'diffuse' receptor system overlaying the skeleton, such that the whole exterior functions as a compound eye (described in Millott, 1968). It has further been proposed that, in the congeneric *Diadema antillarum*, the spine bases could screen off-axis light (Woodley, 1982), forming distinct units analogous to ommatidia.

Performance of simple visual systems can be estimated from an animal's morphology but also by investigating the animal's response to visual stimuli. Behavioural responses provide a conservative measure of stimulus detection as signals which are salient may not elicit a particular response. Specifically, detection acuity (the minimum angular width of a visual stimulus which can be detected) can be used to estimate the spatial resolution: the minimum resolvable distance of components of an object by a complete visual system in the context of the light environment. This methodology has also been applied to taxis in echinoderms by placing individuals at the centre of a circular arena, exposing them to down-welling light and determining whether or not the paths subsequently taken by individuals cluster towards dark visual stimuli of varying angular width, situated on the horizon. This exploits a scototaxis response, occurring in many sea urchins (Holmes, 1912; Adams, 2001), potentially for finding shelter, and is elicited when an animal finds itself displaced into an unsheltered area in daylight. Such methodologies have been applied to echinometrid, strongylocentrotid and diadematid sea urchins

(Al-Wahaibi and Claereboudt, 2017; Blevins and Johnsen, 2004; Yerramilli and Johnsen, 2010), with detection of circular black targets as narrow as 10 deg reported (Yerramilli and Johnsen, 2010) for the purple sea urchin *Strongylocentrotus purpuratus* (Stimpson, 1857). The estimated detection thresholds correspond approximately with the spatial resolution that could be achieved by the animals' spines, which is regarded as support for a diffuse visual system with spines shielding the functional analogue of image pixels (Blevins and Johnsen, 2004; Yerramilli and Johnsen, 2010).

However, the local drop in intensity resulting from the appearance of a dark stimulus could theoretically be detected by a simple directional luminance detector (of sufficient contrast sensitivity). Thus, an animal may detect a broad darkened sector of its field of view, while lacking the capability to resolve the dark object. In addition, estimates of spatial resolution depend on signal contrast and type of pattern. A suitable stimulus should be chosen to achieve maximum precision in estimates of spatial resolution.

Molecular and morphological evidence from *S. purpuratus* suggests that vision is mediated via photoreceptors in the tube feet bases, which are found at the ambulacrum (Ullrich-Lüter et al., 2011). Multiple opsin (animal photopigment) genes have now been identified in the genome of the purple sea urchin *S. purpuratus* (Sodergren et al., 2006), representing all major opsin clades (D'Aniello et al., 2015). The rhabdomeric opsin Sp-opsin 4 (whose orthologues enable vision in fellow echinoderms) is expressed within individual microvillar photoreceptors at the base and apex of the animal's tube feet and the intersecting lateral nerve (Ullrich-Lüter et al., 2011). The basal photoreceptors are located in a cleft of the neural groove of the stalk and are partly screened by the test. From the position of the photoreceptors it is possible to estimate the angular sensitivity, which is the basis for spatial vision.

The aim of this work is to investigate whether or not imaging vision is present in a diadematid urchin, *D. africanum*, and, if so, to determine the approximate resolution used. In addition, we investigate whether this proposed resolution is compatible with either a spine-based or tube-foot-based visual system. *Diadema africanum* was chosen because it is known to exhibit two different photic responses: taxis and a spine-pointing response. *Diadema africanum* and other diadematids have long, hollow moveable spines of two types: primary spines which are sturdy (and some of which are the main locomotory organs) and secondary spines, which are sharp, brittle and venomous (Fig. 1A). They otherwise share a fundamentally similar bauplan to other regular sea urchins (excluding Irregularia).

To behaviourally measure the spatial resolution in *D. africanum*, we investigated the response to visual stimuli of differing sizes in two ways. We measured the taxis of individuals towards visual stimuli of varying angular width along the horizontal plane using isoluminant visual stimuli derived from a difference of Gaussians (DoG) function, which can only be detected by spatially resolving the pattern. Stimuli with black spots or bars on a white background can in principle be detected by simple phototaxis without spatial resolution. We also measured the spine-pointing response to looming visual stimuli of varying angular size. Here, we focused on traditional black stimuli on a bright background because isoluminant stimuli proved inefficient for eliciting behavioural responses. The reason for the larger responses to traditional stimuli may be that they more resemble typical threats for which the spine-pointing response has evolved. Finally, we used X-ray microtomography (μCT) to estimate the resolution expected if the animals utilise a tube foot visual system as proposed for *S. purpuratus*. The spatial resolution for object taxis we determined in *D. africanum* is worse than that reported from other echinoderms.

MATERIALS AND METHODS

Animal collection and husbandry

Wild specimens of *Diadema africanum* were collected in June 2016 in Tenerife, Canary Islands, Spain from the following rocky reef localities: Abades (28°08′31.6″N, 16°26′11.7″W) and Boca Cangrejo (28°24′24.4″N, 16°18′47.4″W). Animals were housed in indoor tanks with regularly replenished and aerated filtered natural seawater. The temperature was maintained at 20°C and natural light from exterior windows entrained the circadian cycle. Green algae (*Ulva* spp.) were provided as a food source. Animals were kept in tanks for between 1 and 10 days, and injured or dying animals were removed daily. Sixty-three individuals were used in these experiments.

Taxis detection task

To assay the object taxis response of *D. africanum* to dark objects of varying width, experimental trials were conducted in which individuals were placed in a lit arena, surrounded by printed patterns containing a printed visual stimulus (Fig. 1B). The animals' trajectories in relation to the stimulus were tracked and compared for differing stimulus treatments.

Arena

Experimental trials were conducted in an arena comprising a cylinder of transparent acrylic sealed to a flat circular base (Fig. 1B). The cylinder had a height of 360 mm and an internal diameter of 495 mm, around which were placed a series of patterned stimuli. This arena was surrounded by a white cylinder to exclude external cues. Above the arena, two Ecotech Radion xr30w aquaria LED lights (PA, USA) were fixed to produce an array of four equidistant clusters of LEDs resulting in broad-spectrum visible illumination (Fig. S1A). The diffuser comprised two sheets of ¾ diffusion paper (Lee Filters 416, Andover, UK; transmission 50%, summed across 400–700 nm) sandwiched between two sheets of Makrolon® (Covestro, Leverkusen, Germany) polycarbonate within a wooden frame. A GoPro HERO 4 black camera was set centrally, directly below these lights and above the centre of the arena, where the lens was directed. The camera was controlled remotely and to record time-lapse videos at a rate of 5 frames s^{-1}. The image distortion caused by the fisheye lens makes the precise measuring of track length difficult away from the centre of the scene but permits accurate estimates of heading direction. The arena was filled with filtered natural seawater, at the same temperature that the animals were housed in (20°C).

Behavioural stimuli

The patterns consisted of greyscale printed images, which were uniform in the vertical plane but in the horizontal plane included stimuli that consisted of dark (black) regions set against a lighter (grey) background. Two pattern types were used (Fig. 1C). In the first case, these pattern used a bar stimulus, in which a solid region of a homogenously black stimulus was presented against a white background. In the second case, the centre of the stimulus was maximally dark, but of increasing reflectance towards the periphery of the stimulus (on the horizontal axis) and reaching the maximum achievable reflectance before darkening into the grey background. The black-level of printing ink pattern was distributed according to a one-dimensional DoG function, in which the secondary Gaussian (the lighter region outside the stimulus) was twice as wide as that

Journal of Experimental Biology (2018) 221, jeb176271. doi:10.1242/jeb.176271

of the primary Gaussian (the dark stimulus) but half the amplitude (see Fig. 1C). The DoG function was defined as:

$$\Gamma_\sigma(x) = \frac{1}{\sigma\sqrt{2\pi}}\, e^{-\frac{(x)^2}{2\sigma^2}} - \frac{1}{2\sigma\sqrt{2\pi}}\, e^{-\frac{(x)^2}{8\sigma^2}}, \qquad (1)$$

where σ is the variance of the primary Gaussian and the variance of the secondary Gaussian is twice σ. The value of x is a numeric scale used to indicate the horizontal position on the printed images with the stimulus centre as the origin. The function $\Gamma_\sigma(x)$ indicated the proportion of the maximum ink value used to shade the printed images at each position on this scale. A scaling factor was used to relate the x-values to physical positions on the printed images, such that the stimulus period was a specified proportion of the printed image width (to correspond to arc width when placed around the cylinder). The stimulus target was defined as the full width at half maximum (half-width) of the dark region of the curve produced by the DoG function (equivalent to 70.5% of the half-width of the primary Gaussian and to 61.1% of the width of the dark region between the zero-crossings). These stimuli are isoluminant with respect to the remainder of the patterns on account of the lighter regions flanking the stimulus, i.e. it is not possible to detect the stimulus by simply comparing the radiance profile of different parts of the arena from the centre without having a spatial resolution equivalent to the arc subtended by the stimulus itself. To ensure that the reflectances of the stimuli were in accordance with the printed shades, the reflectance of a set of printed pieces in 10% increments of shading were measured and integrated over the relevant wavelength range of 450–550 nm (Fig. S1B,C).

The DoG stimuli had an arc width of 29 and 69 deg (defined by the full period of the stimulus, i.e. between the two white maxima) and a target width of 10 and 25 deg, respectively, and these formed the main experimental treatment. The target for the bar stimulus (here, considered equivalent to the period) was large, comprising a 40 deg arc, and this was used to observe whether this signal type elicited a different response to the DoG treatment. Resolution was measured in relation to the full period of the DoG wavelet, in order to relate to other experimental measurements based on the smallest resolvable sine period and, thus, conventional measures of resolution.

Comparison of signals

To evaluate the efficacy of visual signal types to measure spatial resolution, we examined the spatial frequency composition of several signals, including those used herein, to compare the range of spatial frequencies present in each signal, with a period of 10 deg (for clarity). We compare these wavelet signals with a continuous periodic sine. In addition, we compared the relative Michelson contrast (modulation) remaining in the signal image with a period of 30 deg, when convolved with a Gaussian filter. This was used to compare the signal content of the stimulus detectable by receptors of increasing acceptance angle (half-width of the angular sensitivity function) and, thus, deteriorating resolution. The signals we compare are: (i) a periodic sine wave, (ii) a discrete dark bar or spot (for which the period is the width of the bar/spot), (iii) dual bars of equal width and equal but opposite amplitude representing a Haar wavelet, (iv) a piecewise sine wavelet consisting of a negative half-period sine flanked on each side by a positive half-period sine of half the amplitude, and (v) a DoG signal, as described above. Signals iii and iv have been used elsewhere to measure the spatial resolution of an onychophoran (Kirwan et al., 2018b).

Light levels

To ensure that biologically relevant light levels were applied, the animals' natural light environment and that of the setup were measured. The side-welling radiance reflected from the patterns was measured within the complete setup. A calibrated RAMSES ARC-VIS spectroradiometer (TriOS, Germany) was used, positioned 6 cm perpendicular to the grey background of the arena wall (see Fig. S1A). The radiance in the experimental setup over the range 400–700 nm was 0.97×10^{16} quanta m^{-2} s^{-1} sr^{-1} nm^{-1} and, in the blue region (400–500 nm), where the animals are assumed to be most sensitive, the radiance was 1.9×10^{16} quanta m^{-2} s^{-1} sr^{-1} nm^{-1}. The corresponding radiance of the animals' natural light environment was measured in three spectral slots (400–500 nm, 500–600 nm and 600–700 nm) using a calibrated camera (J.S. and D.-E.N., unpublished). On an overcast June day at the sea urchin barren at Boca Cangrejo at a depth of approximately 5 m, the spectral radiance of side-welling light was measured as 2×10^{16} quanta m^{-2} s^{-1} sr^{-1} nm^{-1} averaged over 400–700 nm, and 1.58×10^{16} quanta m^{-2} s^{-1} sr^{-1} nm^{-1} for blue light (400–500 nm). When the habitat radiance was measured, sea urchins at the same site responded to approaching stimuli with their alarm response, indicating that they are responsive at these daylight levels. Given that daytime ambient illumination can vary over more than two log units depending on cloud conditions, our experimental radiances were well within the range of natural daylight.

Trials

In each trial, the animal was placed by hand in the centre of the arena and allowed to move to the periphery. The diffuser and camera were promptly set in place, above the arena, at which point the trial was initiated and recording began. Each trial continued for a maximum of 6 min or until the animal approached the arena wall. A trial was deemed complete if the animal moved at least three-quarters of the radial distance between the centre and arena walls. Trials were conducted in sets of four and the stimulus was moved 90 deg clockwise for each subsequent trial, to negate the influence of any non-visual directional cues. Sets for which there were not four completed trials (e.g. due to a loss of motivation) were excluded from analysis. The base of the arena was cleaned between trial sets with a brush to obscure chemical cues and the water was partially or completely changed, depending on its clarity. Experiments were performed during the daylight period of their entrainment. The frame rate for the recordings was 1 frame s^{-1} (reduced in a few cases).

Analysis

The path that each of the animals took from the centre of the arena to the periphery was tracked using custom software (Smolka et al., 2012) written for MATLAB 9.0 (MathWorks, MA, USA). To represent the bearing taken by the animal from the centre of the arena, the vector of the tracked points which were closest to one quarter (point i) and one half (point ii) of the arena radius from the centre was determined, and the intersection of this vector with the arena wall was recorded. The angular position of this intersection point on the arena wall was used as a measure of the animal's bearing and this was determined in relation to the stimulus' position, i.e. moving in a straight line from the centre to the stimulus would correspond to a heading of 0 rad (0 deg) and the opposite orientation would correspond to π rad (180 deg). To determine whether the taxis response varied as a function of the different stimulus conditions, we compared the response rate using a generalized linear mixed model (glmm). As a metric for response

rate, we assessed success or failure in orientation for each trial by determining whether the bearing fell within the quadrant with the stimulus' centre at its arc midpoint. If so, the animal was considered to have successfully oriented. Mixed effects models were fitted using the package lme4 (Bates et al., 2015) in R, with individual differences of animals included as a random variable to account for pseudoreplication. Models were assessed by direct comparison of Akaike information criterion (AIC) values.

Alarm response detection task

We quantified the spatial resolution of the *D. africanum* alarm response, which occurs as spine pointing: the rapid movement of the sharp, venomous secondary spines. Five animals that had been used in the taxis experiments (regardless of prior performance) were exposed to stimuli displayed on a liquid-crystal display (LCD) screen. The animals were placed in a plastic cone (80 mm depth and 150 mm diameter) affixed centrally to the long side of a glass aquarium (with internal dimensions: 596 mm length×305 mm width×305 mm depth of water; see Fig. 1D). A Pavilion 22cw IPS LED backlit monitor (Hewlett-Packard, CA, USA) was placed flush with the exterior surface of the opposite wall of the aquarium, facing the animals, such that the middle of the screen was located at the centre of the field of view of the animal within the cone. The walls and top of the aquarium were covered with white card to exclude competing stimuli. A sequence of stimuli was then displayed to each animal, consisting of black circles of varying diameter against brighter backgrounds (as well as controls using white circles against dark backgrounds). For each treatment, two versions of the stimulus were applied, one in which the circle appeared suddenly and another in which it loomed over the course of 1 s. Isoluminant stimuli were also tested, but abandoned since they proved far less efficient in eliciting responses.

Five observers were shown videos of the spine-pointing trials in which the stimuli had been spliced out. They were shown training data of responses and non-responses for each animal and asked to record the presence of responses to the stimuli (to which they were blind). The proportions of spine-pointing responses (based on agreement of independent assessment by the observers) for each stimulus and animal were determined. These were used to estimate the spatial resolution threshold using a logistic regression mixed model (with individual animal modelled as a random intercept).

Behavioural estimation of angular sensitivity

The detection tests allowed us to model a range of values within which the widest possible acceptance angle ($\Delta\rho$) could fall, with respect to a plausible range of contrast threshold values. Having determined the detection acuity of *D. africanum* in respect of two different visual tasks, we estimated the angular sensitivity necessitated by the elicited behaviours.

To determine the angular sensitivity that would be required to detect a given stimulus, we modelled how visible the stimulus signal would be to photoreceptors of different acceptance angles. The stimulus image (across a range of widths) was first convolved with a Gaussian spatial filter, the image blur created by the photoreceptor acceptance angle. The modulation of the filtered image was then calculated as a percentage of the Michelson contrast of the unfiltered image, to determine the remaining contrast of the original signal that is still present in the filtered image. Then, for a range of contrast thresholds, we found the narrowest angle subtense of a theoretical receptor at which the stimulus contrast remaining in the image dropped to the threshold value. Thus, by assuming a range of values within which the contrast threshold might fall (as we have not measured contrast sensitivity in this species), we estimate the widest possible acceptance angle of a theorized photoreceptor which could resolve the signal. Therefore, we assumed a contrast sensitivity range, corresponding to a plausible range of contrast thresholds (from 5 to 20%). This range overlaps with the range of maximal contrast-sensitivity thresholds observed in most birds (Lind et al., 2012) and that of the honey bee across most spatial frequencies (Bidwell and Goodman, 1993), but is far less than the maximum observed in humans and certain other vertebrates and insects (O'Carroll and Wiederman, 2014). This was done for both types of stimulus object used (solid bar/spot or DoG), by measuring the change in Michelson contrast over the stimulus, with decreasing visual acceptance angle. This was carried out for the upper and lower ranges of the detection test estimates and a curve was fitted to these points using a smoothing spline in R 3.4.1 (https://www.R-project.org).

The methodology applied here is the same as has been applied to describe the angular sensitivity of the onychophoran *Euperipatoides rowelli* (Kirwan et al., 2018b); however, in those investigations, angular sensitivity and, specifically, the acceptance angle ($\Delta\rho$) are referred to as spatial resolution (by analogy to the resolving capability of the visual system).

Skeleton morphology

To ascertain whether the structure of the neural canal groove of the tube foot pore of *D. africanum* could serve as the visual photoreceptive system, as suggested for *S. purpuratus* (Ullrich-Lüter et al., 2011), we carried out scanning electron microscopy (SEM) and µCT of denuded *D. africanum* tests. Twelve individuals were sacrificed by removal of the Aristotle's lantern, regardless of their performance in trials. To denude the tests, spines were removed manually and the tests were then left in a solution of sodium hypochlorite (7.5×10^{-6} g l^{-1}) in tap water for 3 h and rinsed. Two intact tests were selected and cut to produce sections with intact ambulacra. Several lateral sections were cut from one test with a horizontal diameter of 55 mm and were sputtered with gold in preparation for SEM, which was performed using a Hitachi (Tokyo) SU3500 microscope. For µCT, imaging of a whole test was carried out at 46.5 µm using a Zeiss Xradia XRM520. A section of the ambulacrum from the widest part of the sea urchin, containing four adjacent tube foot pore pairs, was imaged at 3.5 µm resolution at 80 kV from a total of 500 images. Reconstruction of µCT images was carried out using AMIRA 6.0.1 (FEI, Hillsboro, OR, USA), wherein we labelled the putative visual photoreceptive region (hereafter, the receptor group) of each of the tube foot pores.

We estimated the acceptance angle of light entering each of these pores (assuming perfect transmittance through the tube foot, and no transmittance through the combined test and epidermis). Using a custom MATLAB program, we first simulated the paths of over 10,000 equidistant rays towards the section of ambulacrum. We then determined the field of view of these regions by calculating the proportion of rays reaching each receptor and finding the approximate solid angle that these incident rays subtended. To measure the angular aperture, we assumed an approximately circular field of view, and found the resulting angle subtended by incident rays. Furthermore, we measured the inter-receptor angles between the putative tube foot pore receptors. The vector between the mean point of each receptor and the mean point of the incident rays was determined. Inter-receptor angles on the vertical plane (along the tube foot row) were measured from the angles between these vectors for the adjacent receptors. The angle was found between the vector of each receptor and a line perpendicular to the ambulacral midpoint along the same horizontal plane. Inter-receptor

angles with the adjacent receptor horizontally across the ambulacrum were measured by doubling this angle.

We estimated the optical cut-off frequency (ν_{co}) that could be achieved with these receptor groups, by assuming an approximately Gaussian optical transfer function, according to the formula:

$$\nu_{co} = \frac{1}{0.4571\ \theta}, \quad (2)$$

where θ is the angular aperture, and the constant 0.4571 represents the ratio between the half-width of a Gaussian density and the bounds comprising 0.99 of the density (approximating the total angular aperture). In addition, we determined the spine density of the test at eight 2.5 mm increments along the oral–aboral axis by counting the occurrence of spine tubercles in µCT sections to determine the achievable spatial resolution of a visual system screened by spines. As the screening system proposed for *Diadema* makes use of the large spine bases (Woodley, 1982), we counted only pronounced tubercles of >1 mm width present in a given section in order to exclude small secondary spines.

RESULTS

Taxis response

A total of 252 successful trials were used in the taxis experiments, within 63 sets (Table 1; Movie 1, Table S2). The directional vectors taken by the animals in relation to the centre of the stimulus are represented in Fig. 2. The most likely model [Akaike information criterion (AIC) value=317] included an effect of stimulus type but not of stimulus position (model 3; Table 2) and was more likely than the null model (AIC=320), as supported by a likelihood ration test (χ^2=9.6293; P=0.022). Stimulus position is equivalent to the trial order for each animal, due to the stimulus being rotated 90 deg after each trial. For this model (Table 3), the only significant difference in treatment from the control was for the 69 deg DoG stimulus (P=0.0126). No significant difference was found for the 40 deg bar stimulus. No effect of the random variable (i.e. individual effects) occurred in the model and the estimates are consequently identical to the success rates which occurred at each treatment during the trials. The maximal model, which included an interaction of stimulus type and position, did not converge, which may be because this model was parameter rich. We thus omitted this maximal model from our analyses.

To determine whether these data could be treated as distinct data points, we assessed whether the patterns evident for each treatment were recapitulated when the treatments were broken down by trial set (i.e. that individual animals do unduly influence the distribution of data). Plotting the bearings for only the first trial from each trial set (Fig. S2), i.e. the first position, we found that the distributions of bearings were broadly in accordance with the pattern described by the models reported above. In particular, the first trials of the control treatment are not clustered, whereas there is clustering towards the 69 deg DoG stimulus, in keeping with the patterns of the complete data sets. This supports the contention that individual effects and the order of the trials did not influence the data. Consequently, it may be informative to treat the bearings as independent replicates and apply tests of circular uniformity to the bearings (Table 1). In keeping with the results of the mixed model, these tests indicate that there is significant clustering towards the 69 deg DoG stimulus (V-test, P=0.000014), which does not occur towards the control (V-test, P=0.4256) or the 29 deg DoG stimulus (V-test, P=0.4786). As the sample size for the 69 deg DoG stimulus (n=96) is greater than the other treatments, it was possible that statistical power was greater for this treatment, increasing the possibility of a significant result relative to the other treatments. To account for this, we resampled from the 96 observations for the 69 deg DoG stimulus to produce 1000 subsets of 40 observations. We carried out the V-test on each of these subsets, which resulted in an average P-value of 0.02 and a significant result for greater than 89% of the subsets. These tests support the validity of the model. In contrast to the mixed model, the V-test for the 40 deg bar stimulus found significant evidence (P=0.0419) of concentration towards the stimulus. It is thus unclear whether animals are oriented towards the 40 deg bar treatment.

Alarm response to sudden stimuli

To estimate the spatial resolution of the *D. africanum* spine-pointing alarm response, five individuals were exposed to visual stimuli of varying solid angular area (Movie 2, Table S3). The logistic regression mixed model used to analyze these data (Fig. 3) indicated that dark circles subtending solid angular widths of 25 and 44 deg were detectable by *D. africanum*, but those subtending 13 deg were not. When control stimuli, consisting of white circles appearing on black backgrounds, corresponding in size to the experimental stimuli, were applied, the observers never agreed that an alarm response occurred. Of six control stimulus types applied to each of the animals, a maximum of two recorders agreed that an alarm response occurred for a given stimulus event [0.47±0.61 (mean ±s.d.)]. Thus, we expect the false-positive rate (the rate at which the recorders agree that an alarm response occurred, when none took place) for the experimental data to be close to zero. Conversely, estimates of the proportion of correct choices in excess of zero would indicate that an alarm response to the stimulus occurred.

The logistic regression mixed-model estimates of proportion of correct choices (responses to dark stimuli) with respect to the angular width of the stimulus indicate that almost no correct responses occur at an angular width of 13 deg, whereas a response proportion in excess of 0.9 is estimated for an angular width of 44 deg. A correct response proportion in excess of 0.3 is estimated for stimuli of an angular width of 25 deg. On this basis, the detection threshold of stimulus diameter lies within the range of 13–25 deg. The model is considered more likely than the null model (model AIC 68, d.f.=3; null model AIC 125, d.f.=2). To test whether there was a difference between the response to the suddenly appearing and looming stimulus, this variable was included as a fixed effect in the full model. As the AIC for this model (d.f.=6; AIC=59) was

Table 1. Summary of trials and responses conducted to test the detection of a visual stimulus by the sea urchin *Diadema africanum* (α=0.05)

Stimulus	Arc (deg)	*n*	ρ	*V*-test (µ=0) statistic	V test (µ=0) *P*-value	Rayleigh test statistic	Rayleigh test *P*-value
Control	0	44	0.077	0.0503	0.31915	0.0766	0.77470
DoG	29	44	0.011	0.0058	0.47857	0.0107	0.99502
DoG	69	96	0.3	0.2989	0.00001*	0.3001	0.00018*
Bar	40	68	0.188	0.1483	0.04189*	0.1881	0.09016

The mean resultant length (ρ) is a measure of the concentration of the points in a bearing in some direction, as opposed to being uniformly distributed. DoG, difference of Gaussians. *P<0.05.

Journal of Experimental Biology (2018) 221, jeb176271. doi:10.1242/jeb.176271

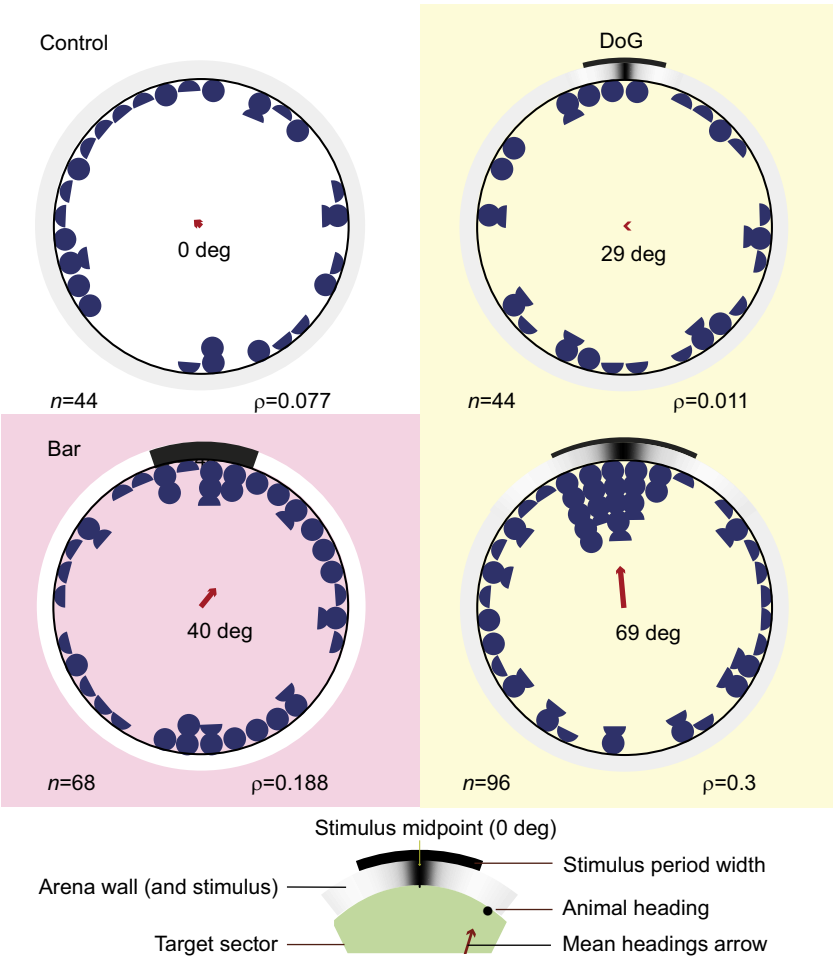

Fig. 2. Object taxis headings taken by specimens of *D. africanum* over multiple trials when exposed to differing visual stimuli. The four large circles are presentations of the arena surrounded by the printed images, with the animal's orientation indicated for each stimulus treatment (red arrow). Each blue semicircle is equivalent to one bearing and each blue circle is equivalent to two bearings. Bearings have been binned in 5 deg increments. The 0 deg position (the stimulus arc midpoint) is at the very top of each diagram. The direction of the red arrow indicates the circular mean orientation and the length of the arrow as a proportion of the arena indicates the mean resultant length (ρ), also indicated to the bottom right of each treatment.

greater than otherwise, this term was excluded (i.e. looming and appearing stimuli were considered together).

Stimulus signals

Our comparison of the frequency content of stimulus signals (Fig. 4A) shows that the DoG signal comprises a narrower band of spatial frequencies than the non-isoluminant black bar (or spot)-type stimulus signal or other isoluminant stimuli. This is especially true at high spatial frequencies, as the DoG does not include high frequency harmonics, whereas even the piecewise sine wavelet does. The periodic sine signal comprises a single spatial frequency and provides an ideal standard. In addition, determining the relative contrast remaining in the image of a 30 deg stimulus with changing receptor acceptance angle based on convolution with a Gaussian filter (Fig. 4B) reveals that the contrast remaining in the discrete signals is generally higher than the continuous signals (which makes detection easier). With large acceptance angles (greater than half of the stimulus period), the DoG pattern is more detectable than the periodic sine wave and the piecewise sine but much less detectable than the discrete stimuli, especially the bar type stimulus. Specifically, contrast drops below 10% for Gaussian filtered images of signals for the sine wave with a period of 30 deg, when the Gaussian half-width subtends 24 deg. This occurs for the piecewise sine wavelet and the DoG when the Gaussian half-width subtends 30 and 38 deg, respectively (and the period subtends 30 deg). It occurs for the dual bars and the bar/spot stimuli at 52 and 75 deg, respectively, indicating a large remaining contrast, relative to the sine, for these discrete signals. Thus, detection of the DoG signal can provide an accurate measure of spatial resolution in comparison to other possible signals, especially dark-spot or bar stimuli.

Table 2. Generalized mixed models applied to success rate of sea urchins in taxis trials

Model	Fixed effects	d.f.	AIC
1	Stimulus type+position+(stimulus type:position)	17	–
2	Stimulus type+position	8	322.3358
3	Stimulus type	5	316.8533
Null	–	5	320.4826

Success was defined as orientation towards the quadrant with the stimulus at the arc midpoint. Individual identity was included as a random effect in each case. The fixed effects – stimulus type and stimulus position – were included as categorical variables. The maximal model (which includes these fixed effects and their interaction) failed to converge. AIC, Akaike information criterion value.

Angular sensitivity

Based on the estimated range for the detection threshold for the taxis response, the widest possible acceptance angle of the theorized

Table 3. Estimated success percentage derived from a generalized mixed effects model for the four treatments

Treatment	*n*	Success (%)
Control	44	20.45
10.4 deg DoG	44	22.73
24.6 deg DoG	96	42.71
40 deg bar	68	30.88

DoG, difference of Gaussians.

Journal of Experimental Biology (2018) 221, jeb176271. doi:10.1242/jeb.176271

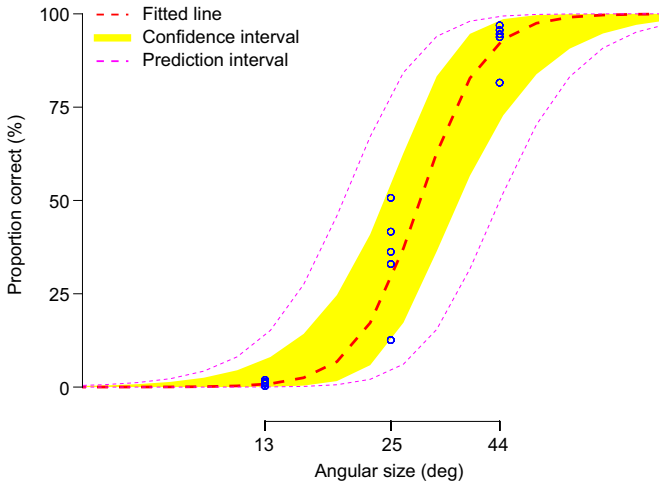

Fig. 3. Spine-pointing response of *D. africanum* to sudden stimuli. Stimuli consisted of dark (black or grey) circles appearing on a white liquid-crystal display (LCD) screen. The diagram indicates the proportion of responses of the animal (n=5) to the stimulus with respect to the log angular size of the stimulus. Responses were evaluated by five recorders who independently assessed the video recordings, and a consensus of all recorders was used to indicate a response.

receptor was modelled as being between 27 and 119 deg, assuming a contrast threshold of between 5 and 20% (Fig. 5). Based on the detection threshold measured for the spine-pointing response, the corresponding acceptance angle of this behaviour was found to be 36 and 213 deg, assuming the same range of contrast threshold.

Skeleton morphology

The neural canal (Smith, 1978a) of the *D. africanum* tube foot is approximately 200 µm in length (Fig. 6). Each neural groove forms part of the peradial tube foot pore and is oriented diagonally orally (downwards) and towards the mid-ambulacrum. From µCT (Movie 3) we can observe that, as per the neural canal groove of *S. purpuratus* (Ullrich-Lüter et al., 2011; Ullrich-Lüter, 2013), those of *D. africanum* are obliquely angled so as to occlude light passing directly through the test to the interior. Data derived from these models are summarized in Table S1. The mean distance between the adjacent neural grooves on the same tube foot row was 6.14±0.44 mm. We found that the mean field of view of each of the putative receptor areas was 3.2±0.29 sr. The field of view of each of the receptor regions was approximately circular (see Fig. S3). Assuming a circular aperture, the mean angular aperture was 92±8 deg. Interreceptor angles between the adjacent pores on the same vertical tube foot row were 8.7, 23 and 8.0 deg from the topmost pore downwards (mean: 13.1±8.2 deg). The mean angle between the midpoint of each receptor aperture and the ambulacral midpoint upon the horizontal axis was 14±1.7 deg. Thus, the interreceptor angle with the adjacent receptor across the ambulacrum was approximately 28 deg. The wide angular aperture we estimate would result in a pronounced sampling overlap.

We estimated the mean spatial cut-off frequency (v_{co}) for these receptors as 0.024±0.002 cycles deg^{-1}. By these estimates, a visual system utilizing these receptor groups could achieve a spatial resolution of 42±4 deg. The reciprocal of the angular aperture provides a more conservative estimate of the cut-off frequency of 0.011±0.001 cycles deg^{-1}. This estimated range of resolution is within the range exhibited by the *D. africanum* alarm response and better than that exhibited by the taxis response. In addition, we

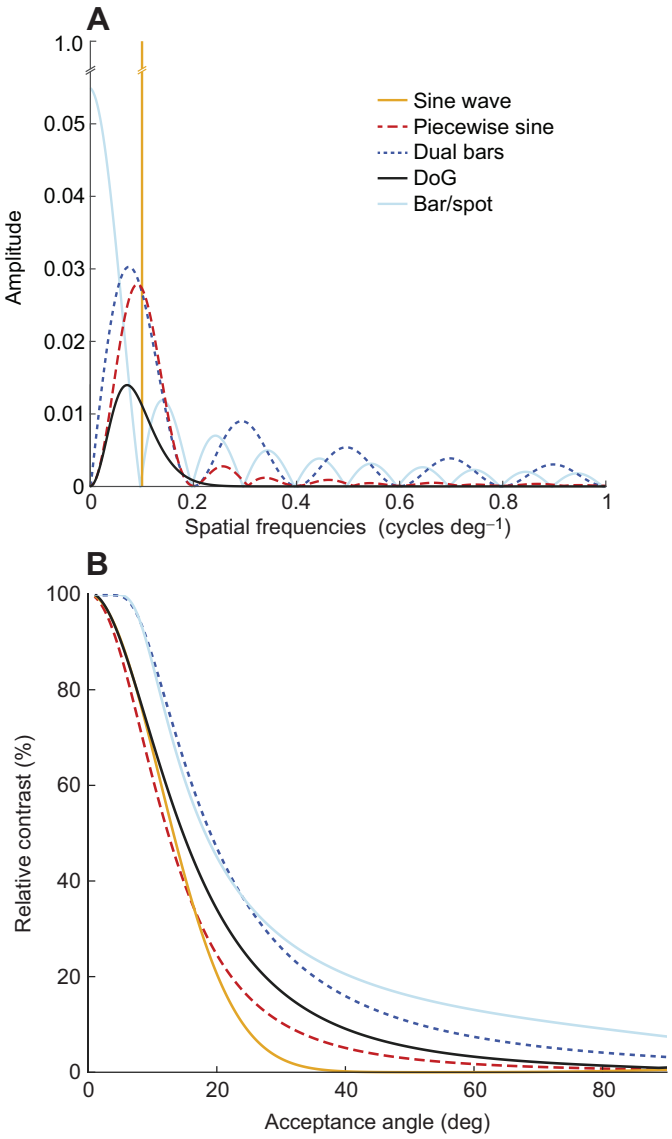

Fig. 4. Properties of visual signals. (A) Fast Fourier transforms of stimulus signal types with a stimulus period of 10 deg to identify the spatial frequencies present in each and their amplitude. (B) Relative contrast (%) remaining in image on convolution with a Gaussian filter for various visual stimulus signals, with a period of 30 deg. Relative contrast is plotted against the acceptance angle of the theoretical receptor. 'Dual bars' indicates the implementation of a Haar wavelet signal, comprising adjacent bars of equal width and equal but opposite amplitude.

found the mean tubercle count to be 12±2.0 from eight horizontal sections (2 mm apart) through the oral–aboral axis. A spine-based visual system could thus achieve a spatial resolution of 60 deg in this plane.

DISCUSSION

Diadema africanum exhibits coarse resolving vision

The spatial resolution exhibited by *D. africanum* during the taxis detection task, however coarse, is nonetheless evidence of resolving vision. Given that animals responded to isoluminant stimuli, this represents, to our knowledge, the first experimental evidence of resolving vision in an echinoid which has been controlled to rule out simple phototaxis (merely moving towards or away from the light). In its simplest form, phototaxis could occur by scanning, using a

Journal of Experimental Biology (2018) 221, jeb176271. doi:10.1242/jeb.176271

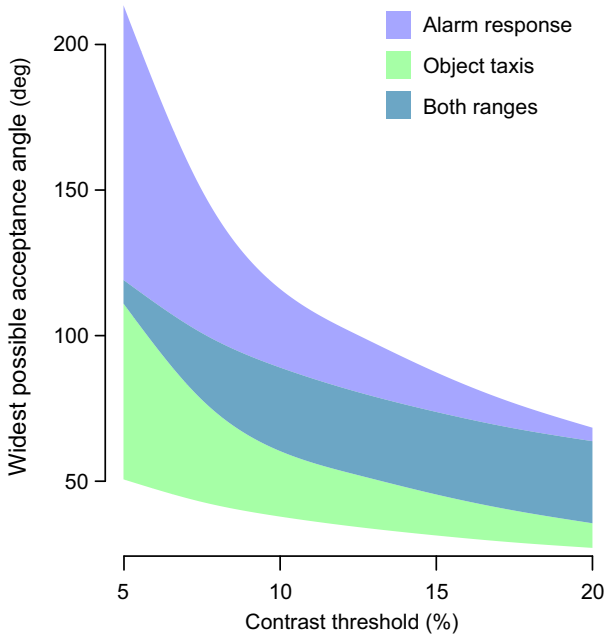

Fig. 5. Angular sensitivity of the taxis response and alarm response estimated for a range of contrast threshold values. For both stimulus types, the range of values between the smallest stimulus to be detected and the largest stimulus not to be detected provide an estimated range for the acceptance angle. As detection is dependent on both resolving power and contrast sensitivity, and as the contrast sensitivity is not known, these ranges were estimated across an ecologically plausible range of contrast threshold values (5–20%). Contrast threshold is the reciprocal of contrast sensitivity expressed as a percentage. The bounds of each range were calculated by simulating the change in contrast over the stimulus, with decreasing visual acceptance angle for a series of contrast threshold values. This was done for the upper and lower ranges of the detection test estimates.

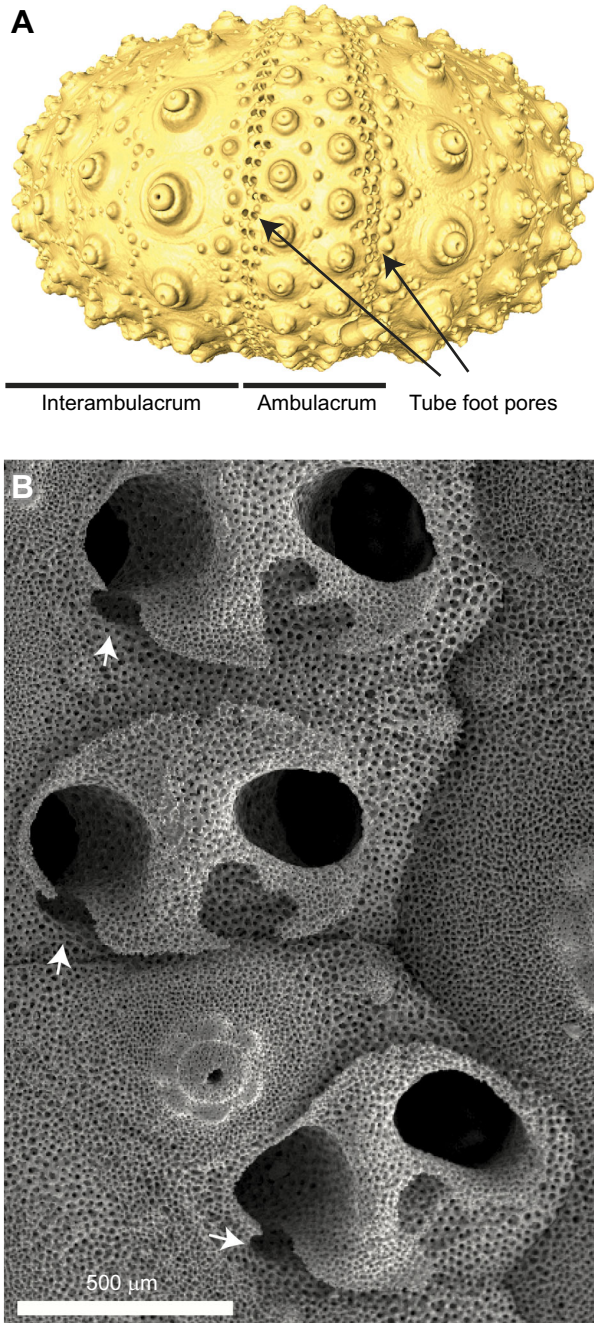

Fig. 6. Tube foot pores of *D. africanum*. (A) Three-dimensional (3D) model of the denuded test (skeleton) of *D. africanum*, derived from X-ray microtomography (µCT). (B) Scanning electron micrograph image of a small region of the test exterior covering the bases of three tube feet. White arrows indicate the position of the neural grooves.

single directional photoreceptor together with body rotation to find the brightest or dimmest direction, an example of which is found in the planktonic trochophore of *Platynereis dumerilii* (Jékely et al., 2008). In contrast, the object taxis, here described from *D. africanum*, requires simultaneous sampling of light from multiple directions, and thus represents true vision. Whether the taxis response in other sea urchin species is truly visual and at what resolution can be further explored.

Several factors could influence the animal's ability to detect the stimuli, resulting in conservative estimates of the detection threshold (i.e. spatial resolution). The detection acuity estimated could constitute a limit of behavioural relevance of the object rather than an absolute detection limit. The condition of some animals may not have been optimal, on account of having been transported from wild habitats and maintained in a laboratory environment. The vertical height of the stimulus and background (and thus the angular subtense in the vertical plane) used for the taxis detection task may influence the response probability. Although *D. africanum* is most active at night (Tuya et al., 2004), experiments were conducted during the day phase of its circadian entrainment in order to compare the visual performance of object taxis and defensive behaviour under the same conditions. It is nonetheless possible that the animals' response rate may differ with a different circadian entrainment. Although the evocation of the alarm response was very robust, this response was not conclusively demonstrated to be visual through the use of isoluminant spatial stimuli. However, the animals were restrained in plastic cones in these experiments and could not use body rotation to determine the position of a luminance minimum. Moreover, the response of the secondary spines to stimulus in the urchin is not general across the body surface but is localized to the sector directed towards the stimulus (Movie 2). This leaves true spatial vision as the only possible explanation for the spine-pointing response, in the absence of scanning behaviour (Nilsson, 2009).

Despite differences in experimental methodology and the behavioural paradigm between the two detection tasks, the proposed ranges of spatial resolution for these behavioural tasks overlap. Thus, the same visual system, optimized to the same or a

similar range of spatial frequencies, could be used for both (without the need for different pathways for neural processing). Given that multiple opsin pigments are expressed by sea urchins, it is possible that different systems, utilizing different photoreceptor systems, are used for different components of the visual repertoire but a single system is the more parsimonious solution.

Regarding the object taxis discrimination task, it is surprising that much clearer evidence was found for orientation towards the 69 deg isoluminant DoG stimulus than the 40 deg bar stimulus, given that there is a much greater local contrast in the case of the bar stimulus and greater amplitude at low spatial frequencies (Fig. 4). However, it is possible that, on account of spatial filtering, the bar stimulus may be less detectable than the DoG signal or that motivation may differ for these different signal types, for reasons related to their ecology. Furthermore, it is possible that, in the experimental context, the response to the bar stimulus may not be robust, which makes it difficult to assess to what extent stimulus detection is occurring for this signal type. The equivalent, but reverse, result was observed with the spine-pointing response, which was robust for black dot stimuli but hard to evoke with isoluminant stimuli. Here, it is possible that the system is tuned to the high contrast of threats appearing against bright down-welling light.

The ecological role of vision in sea urchins

Object taxis via coarse resolving vision could be used for general habitat-finding behaviours, such as locating sections of rocky reef habitat, or perhaps dark patches of algae therein, as a food source. Similar use of coarse spatial vision is used by the crown-of-thorns starfish (Petie et al., 2016) and the blue sea star (Garm and Nilsson, 2014). It is quite possible that sea urchins use visually guided habitat selection in more sophisticated ways than for just moving towards objects in an otherwise empty surrounding. Natural situations similar to that of our taxis experiments would be if an animal becomes displaced by strong currents and finds itself in a sand flat next to suitable rocky structures. A potential and more general role of object taxis is the identification of crevice microhabitats upon the rocky substrate (that these animals frequently inhabit), which increases the diadematid's defensive capabilities due to better purchase and reduced exposure. It is then possible that object contrast and spatial frequencies are used in a more complex way than what we have revealed by our experiments.

The spine-pointing response of diadematids to appearing stimuli is obviously used as a defence against potential attackers. Adult *D. africanum* is preyed upon by durophagous fish (Clemente et al., 2010, 2011), and *Diadema* species are also preyed upon by gastropods and decapods (Muthiga and McClanahan, 2013). It was noted during experimental trials that large individuals were not always motivated to respond via object taxis at all, which may be a consequence of limited predation pressure. *D. africanum* becomes invulnerable to predation on reaching a test diameter of around 40 mm (Clemente et al., 2007), which is approximately the size of the largest individuals used here.

Resolving vision is redundant for non-visual photoreception tasks such as circadian entrainment, shadow detection or non-visual phototaxis (Nilsson, 2013; Nilsson and Bok, 2017), which may be achieved in the sea urchin via distinct receptors. Sea urchin vision could, however, contribute to guiding body orientation upon the substrate or simple orientation with respect to a landmark. The optical resolving power of *D. africanum* vision as evidenced here is derisively poor for advanced behaviours, which involve individual recognition of conspecifics or other small objects. Nonetheless, vision could contribute to aggregation of conspecifics, given their distinctive dark colour that may improve the attractiveness of an already heavily populated area. Diadematids tend to form aggregations when exposed (Pearse and Arch, 1969) and vision could thereby contribute to predator defence. Although *Diadema* species are gonochoristic, they are outwardly sexually monomorphic (Muthiga and McClanahan, 2013), which precludes a visual component to sex recognition. However, spawning is synchronized between both sexes from waning to new moon (Hernández et al., 2011); therefore, visual recognition of an aggregation of adults could increase fertilization during the reproductive period.

As stated above, *D. africanum* and its congenerics are of considerable ecological importance. *Diadema africanum* has an important role in influencing the composition of algal assemblages and, due to reduced predation, has formed extensive sea urchin barrens in the Canary Islands (Hernández et al., 2008). *Diadema antillarum* plays an important ecological role in Caribbean coral reefs and is beneficial to coral growth at intermediate densities (Sammarco, 1980) but has not recovered from a mass mortality event in 1983 (Lessios, 2016). An improved understanding of the sensory biology of these animals may assist with their control or conservation.

Isoluminant narrowband signals are preferable as visual stimuli

As mentioned, the ideal visual stimulus to measure spatial resolution is a periodic sine wave grating (Fig. 4). This is because it is composed of a single spatial frequency, which makes the detection threshold of a task directly relatable to resolution. Stimuli of this kind of signal are widely used in vision experiments, such as when eliciting an optomotor response. However, such methods are not amenable to all behavioural tasks or to every species. For directional tasks, such as orientation, a single period function may be more suitable. Conventionally, this has involved bar or spot stimuli, with a uniform intensity, which form a high-contrast edge against the background. As is evident from our comparison of stimulus signal types (Fig. 4), such stimuli have limitations in comparison to isoluminant signals, especially those lacking a discrete edge. Of the wavelet stimuli we compared (excluding the sine), the continuous wavelets performed best, especially the DoG signal, in terms of the narrow range of spatial frequencies present.

Sea urchin vision could be mediated by the tube feet

The range of estimates of spatial resolution from the taxis detection task of *D. africanum* is in the same range as our estimate of what resolution could be achieved by a tube foot pore receptor system in this species. The range of estimates for the alarm response is worse but could, nonetheless, be accommodated by the same system. This lends credence to the existence of such a system (analogous to that which has been proposed for *S. purpuratus*) for diadematids and potentially other euechinoids. As noted by Ullrich-Lüter (2013), the observation that photic sensitivity of the *D. africanum* test is greatest at the ambulacral margin and least at the interambulacrum is consistent with a tube-foot-based visual system (Millott and Yoshida, 1960), and the possibility of such a system has been suggested for *Diadema* (Millott and Coleman, 1968). The skeleton of *D. africanum* is thinner than that of *S. purpuratus* but the combined test and dark dermal layers could, nonetheless, provide effective screening. The paucity of tube foot pores in the horizontal plane ultimately limits sampling frequency and could contribute to the reduced spatial resolution evident from the taxis detection task in comparison with the alarm response detection task. The sampling overlap between adjacent receptors in both axes could contribute to increased sensitivity. A tube-foot-pore-based visual system has the

advantage of being static in relation to the animal and its whole body movement, whereas a system which relied on screening by the spines would be subject to the erratic movement of these appendages. To support the idea that such a system is present in *D. africanum*, the localized expression of a visual pigment (most parsimoniously, the orthologue of *S. purpuratus* Sp-opsin 4) ought to be identified associated with the tube foot pore neural groove. Notwithstanding this, the proposed spatial resolution of behaviour, and morphology, taken on their own, are also consistent with the spine screening hypothesis. However, other lines of evidence would need to be identified to further corroborate this.

As mentioned above, it is possible that multiple photoreceptor systems are used in urchin vision for different behavioural tasks. Moreover, in addition to the rhabdomeric photopigment, Sp-opsin 4, identified in the tube feet region, the ciliary photopigment gene *Sp-opsin 1* is expressed in cells throughout the epidermis of *S. purpuratus* (Ullrich-Lüter, 2013; Ullrich-Lüter et al., 2013). If there is a similar arrangement in *D. africanum*, and given a screening mechanism to provide resolution, a visual system based on this photopigment could be responsible for certain visual tasks.

The neural canal is a general feature of sea urchin tube foot pores, although the size and morphology can vary (Smith, 1978a). Echinoids appeared in the Ordovician (Smith and Savill, 2001) and the major groups of regular sea urchins radiated in the lower Mesozoic. Some aspects of morphology appear to have altered little structurally in the interim. Jurassic sea urchins closely resemble the modern range of forms (Smith, 1980) and their tube feet pores had similar neural canals (Smith, 1978b). Thus, if sea urchins use this system for vision, the morphological prerequisites have been in existence since at least the lower Mesozoic and possibly the late Ordovician.

Conclusions

We find that *D. africanum* responds by taxis towards isoluminant wavelet stimuli with a spatial resolution of 29–69 deg, corresponding to an acceptance angle of 38–89 deg, assuming a contrast threshold of 10%. We also find that *D. africanum* displays a spine-pointing response to appearing black circles with a resolution of between 13 and 25 deg, corresponding to an acceptance angle of 60–116 deg, assuming a contrast sensitivity of 10. The resolution which we predict from a tube foot pore-based visual detector (42 deg) is consistent with this range of values.

Acknowledgements

The authors thank Esther Ullrich-Lüter for contributing to the idea for this project and for comments on the manuscript, Todd Oakley for contributing to experimental design, Sam Walmsley for his assistance with preliminary experiments, Pierre Tichit and Gavin Taylor for their assistance with AMIRA and morphological measurements, Klara Kihlström, David Szakal, Viktor Håkansson, Ajinkya Dahake and Lisa Schilha for observing sea urchin alarm responses, and Stephen Hall and the Lund University 4D lab for carrying out µCT.

Competing interests

The authors declare no competing or financial interests.

Author contributions

Conceptualization: J.D.K., M.J.B., J.S., D.-E.N.; Methodology: J.D.K., M.J.B., J.S., D.-E.N.; Software: J.S.; Formal analysis: J.D.K., J.S., J.J.F.; Investigation: J.D.K., M.J.B., J.C.H.; Resources: J.C.H., D.-E.N.; Writing - original draft: J.D.K.; Writing - review & editing: J.D.K., M.J.B., J.S., J.J.F., J.C.H., D.-E.N.; Visualization: J.D.K.; Supervision: D.-E.N.; Project administration: D.-E.N.; Funding acquisition: D.-E.N.

Funding

This project was funded by the Knut and Alice Wallenberg Foundation ('Ultimate Vision' to D.-E.N.) and by the Swedish Research Council (Vetenskapsrådet; grant to D.-E.N.).

Data availability

Additional data are made available at the Dryad repository doi:10.5061/dryad.6vn9658 (Kirwan et al., 2018a). These comprise MATLAB scripts to create stimulus patterns and to determine what spatial resolution can detect a given signal as well as the images used in the 3D reconstruction.

Supplementary information

Supplementary information available online at http://jeb.biologists.org/lookup/doi/10.1242/jeb.176271.supplemental

References

Adams, N. L. (2001). UV radiation evokes negative phototaxis and covering behavior in the sea urchin *Strongylocentrotus droebachiensis*. *Mar. Ecol. Prog. Ser.* **213**, 87-95.

Al-Wahaibi, M. K. and Claereboudt, M. R. (2017). Extraocular vision in the sea urchin *Diadema setosum*. *Mar. Freshw. Behav. Physiol.* **50**, 1-10.

Bates, D. M., Mächler, M., Bolker, B. and Walker, S. (2015). Fitting linear mixed-effects models using lme4. *J. Stat. Softw.* **67**, 1-48.

Bidwell, N. J. and Goodman, L. J. (1993). Possible functions of a population of descending neurons in the honeybee's visuo-motor pathway. *Apidologie* **24**, 333-354.

Blevins, E. and Johnsen, S. (2004). Spatial vision in the echinoid genus Echinometra. *J. Exp. Biol.* **207**, 4249-4253.

Bok, M. J., Capa, M. and Nilsson, D.-E. (2016). Here, there and everywhere: the radiolar eyes of fan worms (Annelida, Sabellidae). *Integr. Comp. Biol.* **56**, 784-795.

Bok, M. J., Porter, M. L., Ten Hove, H. A., Smith, R. and Nilsson, D.-E. (2017a). Radiolar eyes of serpulid worms (Annelida, Serpulidae): structures, function, and phototransduction. *Biol. Bull.* **233**, 39-57.

Bok, M. J., Porter, M. L. and Nilsson, D.-E. (2017b). Phototransduction in fan worm radiolar eyes. *Curr. Biol.* **27**, R698-R699.

Clemente, S., Hernández, J. C., Toledo, K. and Brito, A. (2007). Predation upon Diadema aff. antillarum in barren grounds in the Canary Islands. *Sci. Mar.* **71**, 745-754.

Clemente, S., Hernández, J. C., Rodríguez, A. and Brito, A. (2010). Identifying keystone predators and the importance of preserving functional diversity in sublittoral rocky-bottom areas. *Mar. Ecol. Prog. Ser.* **413**, 55-67.

Clemente, S., Hernández, J. C. and Brito, A. (2011). Context-dependent effects of marine protected areas on predatory interactions. *Mar. Ecol. Prog. Ser.* **437**, 119-133.

D'Aniello, S., Delroisse, J., Valero-Gracia, A., Lowe, E. K., Byrne, M., Cannon, J. T., Halanych, K. M., Elphick, M. R., Mallefet, J., Kaul-Strehlow, S. et al. (2015). Opsin evolution in the Ambulacraria. *Mar. Genomics* **24**, 177-183.

Garm, A. Nilsson, D.-E. (2014). Visual navigation in starfish: first evidence for the use of vision and eyes in starfish. *Proc. Biol. Sci.* **281**, 20133011.

Hernández, J. C., Clemente, S., Sangil, C. and Brito, A. (2008). The key role of the sea urchin *Diadema aff. antillarum* in controlling macroalgae assemblages throughout the Canary Islands (eastern subtropical Atlantic): an spatio-temporal approach. *Mar. Environ. Res.* **66**, 259-270.

Hernández, J. C., Clemente, S. and Brito, A. (2011). Effects of seasonality on the reproductive cycle of *Diadema aff. antillarum* in two contrasting habitats: implications for the establishment of a sea urchin fishery. *Mar. Biol.* **158**, 2603-2615.

Holmes, S. J. (1912). Phototaxis in the sea urchin, *Arbacia punctulata*. *J. Anim. Behav.* **2**, 126-136.

Jékely, G., Colombelli, J., Hausen, H., Guy, K., Stelzer, E., Nédélec, F. and Arendt, D. (2008). Mechanism of phototaxis in marine zooplankton. *Nature* **456**, 395-399.

Johnsen, S. and Kier, W. M. (1999). Shade-seeking behaviour under polarized light by the brittlestar *Ophioderma brevispinum* (Echinodermata: Ophiuroidea). *J. Mar. Biol. Assoc. UK* **79**, 761-763.

Kirwan, J. D., Bok, M. J., Smolka, J., Foster, J. J., Hernandez, J. C. and Nilsson, D. (2018a). Data from: The sea urchin Diadema africanum uses low resolution vision to find shelter and deter enemies. Dryad Digital Repository. https://doi.org/10.5061/dryad.6vn9658

Kirwan, J. D., Graf, J., Smolka, J., Mayer, G., Henze, M. J. and Nilsson, D.-E. (2018b). Low resolution vision in a velvet worm (Onychophora). *J. Exp. Biol.* **221**, jeb175802.

Lawrence, J. M. (1976). Covering response in sea urchins. *Nature* **262**, 490-491.

Lessios, H. A. (2016). The great *Diadema antillarum* die-off: 30 years later. *Ann. Rev. Mar. Sci.* **8**, 267-283.

Lind, O., Sunesson, T., Mitkus, M. and Kelber, A. (2012). Luminance-dependence of spatial vision in budgerigars (*Melopsittacus undulatus*) and Bourke's parrots (*Neopsephotus bourkii*). *J. Comp. Physiol. A Neuroethol. Sensory Neural Behav. Physiol.* **198**, 69-77.

Millott, N. (1955). The covering reaction in a tropical sea urchin. *Nature* **175**, 561-561.

Millott, N. (1968). The dermal light sense. In *Invertebrate Photoreceptors*, Symposia of the Zoological Society of London, No. 23 (ed. J. D. Carthy and G. E. Newell), pp. 1–36. London: Academic Press.
Millott, N. and Coleman, R. (1969). The podial pit – a new structure in the echinoid *Diadema antillarum* Philippi. *Z. Zellforch. Microsk. Anat.* **95**, 187-197.
Millott, N. and Takahashi, K. (1963). The shadow reaction of *Diadema antillarum* Philippi. IV. Spine movements and their implications. *Philos. Trans. R. Soc. B Biol. Sci.* **246**, 437-469.
Millott, N. and Yoshida, M. (1960). The shadow reaction of *Diadema Antillarum* Philippi: I. the spine response and its relation to the stimulus. *J. Exp. Biol.* **37**, 363-375.
Mortensen, T. (1940). Aulodonta, with additions to vol. 2 (Lepidocentroida and Stirodonta). *A Monogr. Echinoidea* **3**, 1-197.
Muthiga, N. A. and McClanahan, T. R. (2013). Diadema. In *Sea Urchins: Biology and Ecology* (ed. J. M. Lawrence), pp. 257-274. Elsevier.
Nilsson, D.-E. (2009). The evolution of eyes and visually guided behaviour. *Philos. Trans. R. Soc. Lond. B. Biol. Sci.* **364**, 2833-2847.
Nilsson, D.-E. (2013). Eye evolution and its functional basis. *Vis. Neurosci.* **30**, 5-20.
Nilsson, D.-E. and Bok, M. J. (2017). Low-resolution vision—at the hub of eye evolution. *Integr. Comp. Biol.* **26**, 47-66.
O'Carroll, D. C. and Wiederman, S. D. (2014). Contrast sensitivity and the detection of moving patterns and features. *Philos. Trans. R. Soc. Lond. B. Biol. Sci.* **369**, 20130043.
Pearse, J. S. and Arch, S. W. (1969). The aggregation behavior of diadema (Echinodermata, Echinoidea). *Micronesica* **5**, 165-171.
Petie, R., Hall, M. R., Hyldahl, M. and Garm, A. (2016). Visual orientation by the crown-of-thorns starfish (Acanthaster planci). *Coral Reefs* **35**, 1-12.
Rodríguez, A., Hernández, J. C., Clemente, S. and Coppard, S. E. (2013). A new species of *Diadema* (Echinodermata: Echinoidea: Diadematidae) from the eastern Atlantic Ocean and a neotype designation of *Diadema antillarum* (Philippi, 1845). *Zootaxa* **3636**, 144-170.
Sammarco, P. W. (1980). *Diadema* and its relationship to coral spat mortality: Grazing, competition, and biological disturbance. *J. Exp. Mar. Bio. Ecol.* 45, 245-272.
Smith, A. B. (1978a). A functional classification of the coronal pores of regular echinoids. *Paleontology* **21**, 759-789.
Smith, A. B. (1978b). A comparative study of the life style of two Jurassic irregular echinoids. *Lethaia* **11**, 57-66.
Smith, A. B. (1980). The structure, function and evolution of tube feet and ambulacral pores in irregular echinoids. *Palaeontology* **23**, 39-83.
Smith, A. B. and Savill, J. J. (2001). *Bromidechinus*, a new Ordovician echinozoan (Echinodermata), and its bearing on the early history of echinoids. *Earth Environ. Sci. Trans. R. Soc. Edinburgh* 92, 137-147.
Smolka, J., Baird, E., Byrne, M. J., El Jundi, B., Warrant, E. J. and Dacke, M. (2012). Dung beetles use their dung ball as a mobile thermal refuge. *Curr. Biol.* **22**, R863-R864.
Sodergren, E., Weinstock, G. M., Davidson, E. H., Cameron, R. A., Gibbs, R. A., Angerer, R. C., Angerer, L. M., Arnone, M. I., Burgess, D. R., Burke, R. D. et al. (2006). The genome of the sea urchin *Strongylocentrotus purpuratus*. *Science* **314**, 941-952.
Speiser, D. I., Eernisse, D. J. and Johnsen, S. (2011). A chiton uses aragonite lenses to form images. *Curr. Biol.* **21**, 665-670.
Stimpson, W. (1857). *The Crustacea and Echinodermata of the Pacific shores of North America*. Cambridge, MA: H. O. Houghton & Co.
Tuya, F., Martin, J. A. and Luque, A. (2004). Patterns of nocturnal movement of the long-spined sea urchin *Diadema antillarum* (Philippi) in Gran Canaria (the Canary Islands, central East Atlantic Ocean). *Helgol. Mar. Res.* **58**, 26-31.
Ullrich-Lüter, E. M. (2013). Morphological and molecular studies on photoreceptors in Echinodermata. *PhD Thesis*. Berlin: Freie Universität Berlin.
Ullrich-Lüter, E. M., Dupont, S., Arboleda, E., Hausen, H. and Arnone, M. I. (2011). Unique system of photoreceptors in sea urchin tube feet. *Proc. Natl. Acad. Sci. USA* **108**, 8367-8372.
Ullrich-Lüter, E. M., D'Aniello, S. and Arnone, M. I. (2013). C-opsin expressing photoreceptors in echinoderms. *Integr. Comp. Biol.* **53**, 27-38.
Woodley, J. D. (1982). Photosensitivity in Diadema antillarum: does it show scototaxis? In Echinoderms, proceedings of the International Conference, Tampa Bay, 14-17 September 1981 (ed. J. M. Lawrence), p. 61. Rotterdam: A.A. Balkema.
Yamamoto, M. and Yoshida, M. (1978). Fine structure of the ocelli of a synaptid holothurian, *Opheodesoma spectabilis*, and the effects of light and darkness. *Zoomorphologie* **90**, 1-17.
Yerramilli, D. and Johnsen, S. (2010). Spatial vision in the purple sea urchin *Strongylocentrotus purpuratus* (Echinoidea). *J. Exp. Biol.* **213**, 249-255.
Yoshida, M. (1956). On the light response of the chromatophore of the sea-urchin, *Diadema setosum* (Leske). *J. Exp. Biol* **33**, 119-123.
Yoshida, M. (1966). Photosensitivity. In *Physiology of Echinodermata* (ed. R. A. Boolootián), pp. 435-464. New York: Wiley Interscience.
Yoshida, M. and Millott, N. (1959). Light sensitive nerve in an echinoid. *Experientia* **15**, 13-14.
Yoshida, M., Takasu, N. and Tamotsu, S. (1984). Photoreception in Echinoderms. In *Photoreception and Vision in Invertebrates* (ed. M. A. Ali), pp. 743-771. Boston, MA: Springer.